A particle based approach for improved resolution PIV and TOMO-PIV based on the Coherent Point Drift and the Affine Least-Squares Transformation

B. Mercier[1,*], L. Thomas[1], B. Tremblais[2], L. David[1],

1: Institut P', CNRS, Univ. de Poitiers, ISAE-ENSMA - UPR 3346, SP2MI, Poitiers, France
2: Université de Poitiers, Univ. Limoges, CNRS, XLIM, Poitiers, France
*Corresponding author: bertrand.mercier@univ-poitiers.fr

Keywords: 2D2C PIV, 3D3C PIV, Coherent Point Drift.

ABSTRACT

Particle Image Velocimetry (PIV) is a widely used method for flow diagnostics, but there is still potential for improvement, particularly in terms of velocity gradient estimation and computational cost when considering three-dimensional problems. This paper presents a framework that combines a Particle Tracking Velocity (PTV) approach with local gradient-based Eulerian reconstruction to improve PIV performance. The approach uses the Coherent Point Drift (CPD) method for particle pairing and introduces the Affine Least-Squares Transformation (ALST) for local deformation gradient estimation. The CPD method consists of pairing particles whose positions at two successive instants have been obtained from the images. The ALST estimates local deformation gradients, allowing the Eularian reconstruction of the velocity field. The effectiveness of the proposed method compared to traditional PIV algorithms is demonstrated by synthetic test cases in both 2D and 3D configurations. In 2D cases, the CPD+ALST approach outperforms standard PIV methods, especially in capturing local velocity gradients. In 3D cases, comparisons with TOMO-PIV show the improved performance of CPD+ALST in the context of locally large velocity gradients. However, the linear nature of ALST makes it less efficient than quadratic binning techniques. The study demonstrates the potential of CPD+ALST to improve velocity field reconstruction in complex flows.

1. Introduction

Particle Image Velocimetry, especially in two dimensions, is one of the most widely used method for flow diagnostics, and has benefited from long-terms developments summarized for example in Raffel et al. (2018). Although the method is undoubtedly mature, there is still room for improvement, one of which is the focus of this contribution. In particular, provided that the particles can be identified individually in the images, particle tracking velocity (PTV) schemes can be applied

(see Dabiri & Pecora (2020) for details), and in particular recent developments in two-pulse PTV techniques (Novara et al. (2023); Mercier et al. (2023)) that have shown that particles can be tracked from one frame to another with a relatively high density. However, a comparison of PIV and PTV results often favors PIV techniques when the measurement is not time-resolved. Thanks to a 75% overlap and a reasonably narrow weighting function, the resolution of PIV vector fields can indeed approach the mean distance between particles. The major drawback of correlation-based methods is the computational cost, especially when added to a three-dimensional tomographic reconstruction, and the filtering of the high frequencies.

In this contribution the authors attempt to demonstrate the possibility of improving the performance of PIV, both in terms of computational cost and velocity gradient estimation, with a unique framework for 2- or 3-dimensional problems. This is achieved by combining a PTV approach and a local gradient based Eulerian reconstruction. The PTV is performed using the Coherent Point Drift (CPD) method introduced by Myronenko & Song (2010) and recently adapted by the authors for fluid mechanics applications (Mercier et al. (2023)). The CPD allows to identify pairs of particles between two consecutive images with a relatively low error rate. Beyond the use of CPD, the novelty of this contribution is the coupling between the CPD and an Eulerian reconstruction, introduced as to be the "Affine Least-Squares Transformation" (ALST) by the authors. The ALST consists in estimating the local deformation gradient tensor $\mathbf{F}(\mathbf{x}, t)$ at any arbitrary position from the pairs of particles identified by the CPD. This local nature allows the method to be less computational intensive than other global data binning methods (Gesemann et al. (2016); Sperotto et al. (2022)).

The CPD and the ALST are briefly introduced in the next sections. A comparison between PIV and the present results is then presented for two 2-dimensional test cases based on realistic synthetic images. A comparison with the binning method implemented in Davis 10.2, TOMO-PIV and the present method is then proposed for two 3-dimensional cases.

2. Coherent Point Drift

The Coherent Point Drift (CPD) method, first introduced in 2006 by Myronenko (Myronenko et al. (2006); Myronenko & Song (2010)), is a robust point-set registration algorithm used to align two sets of points in space. Originally developed for computer vision applications, CPD has been successfully adapted to fluid mechanics contexts as demonstrated in Mercier et al. (2023, 2024). In double-frame velocimetry, CPD aligns particles detected from the images associated with frame 1 (source points) with those from frame 2 (target points). The coordinates of these particles are respectively represented as $\mathbf{Y} \in \mathbb{R}^{M \times D}$ and $\mathbf{X} \in \mathbb{R}^{N \times D}$, where $D = 2$ or 3 is the dimension of the problem.

CPD performs this alignment by determining a geometrical transformation $\mathcal{T}(\mathbf{Y}, \boldsymbol{\theta})$ that maxi-

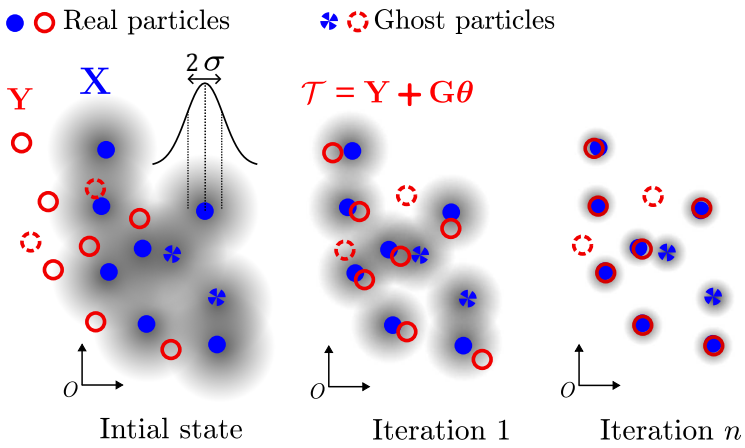

Figure 1. Working principle of the CPD. The point sets $\mathbf{X}$ (•) and $\mathbf{Y}$ (○) are shown in their initial states on the left. For iteration 1 and n, the point sets are $\mathbf{X}$ and $\mathcal{T}(\mathbf{Y}, \boldsymbol{\theta})$ (○). The shaded area represents the influence region of $\mathbf{X}$ for the Gaussian Mixture Model. Figure reproduced from Mercier et al. (2024)

mizes the correspondence between the transformed source points $\tilde{\mathbf{Y}} = \mathbf{Y} + \mathcal{T}(\mathbf{Y}, \boldsymbol{\theta})$ and the target points $\mathbf{X}$. The method handles rigid, affine, and non-rigid deformations, with the non-rigid variant being the most effective for tracking particles in turbulent flows. This transformation is modeled using a Gaussian Mixture Model (GMM), where the centroids are aligned with the source points, and the Gaussians are weighted by parameters $\boldsymbol{\theta}$. The optimization involves minimizing a negative log-likelihood function, which in its simplest form is:

$$E(\boldsymbol{\theta}, \sigma) = -\sum_{n=1}^{N} \log \sum_{m=1}^{M} e^{-\frac{||X_n - Y_m - \mathcal{T}(Y_m, \boldsymbol{\theta})||^2}{2\sigma^2}}. \tag{1}$$

The solution is obtained iteratively using an Expectation-Maximization (EM) algorithm which is illustrated in Figure 1. Initially, σ is estimated, and $\boldsymbol{\theta}$ is optimized to ensure spatial coherence in the deformation. Subsequently, σ is updated to reflect the distance between $\mathbf{X}$ and the updated $\tilde{\mathbf{Y}}$. Through successive iterations, σ decreases, helping to separate unpaired particles from the optimization problem. Convergence results in source particles close to target particles being paired, while those without close neighbors are identified as outliers.

For more detailed information on the original method, see Myronenko & Song (2010), and for the adaptations specific to particle tracking, refer to Mercier et al. (2024).

3. Affine Least-Squares Transformation

The Affine Least-Squares Transformation consists in assuming that the transformation $\zeta_{t_0}^{t_1}$ that define the displacements field of the particles at time t_0 to the time t_1 is only a function of the local deformation gradient tensor, $\mathbf{F}(\mathbf{x_0}, t)$, and the displacement $\mathbf{U} = [U, V, W]'(\mathbf{x_0})$ at a reference posi-

tion $\mathbf{x_0}$ given

$$\zeta_{t_0}^{t_1}(\mathbf{x}, t) = \mathbf{U}_{\mathbf{x_0}} + (\mathbf{F}(\mathbf{x_0}, t) - \mathbf{I})(\mathbf{x} - \mathbf{x_0}) \tag{2}$$

where $\mathbf{I}$ is the identity matrix. The partial derivatives that constitute the tensor $\mathbf{F}$ and the local velocity can be estimated from a set of known displacements in the vicinity of the considered reference position $\mathbf{x_0}$, here corresponding to the position of the particle to be advected. The know displacements $[U_p, V_p, W_p]'$ of the neighbor particle pair p are obtained during the application of the CPD. The problem can be written in the form of a linear system, and is solved in a least-squares sense with

$$\tilde{\mathbf{x}} = \text{argmin}(\ \|\mathbf{A}\mathbf{x} - \mathbf{b}\|_2^2) \tag{3}$$

where $\mathbf{A}$ contains the positions of the particle p $[X_pY_pZ_p]' = [x_py_pz_p]' - \mathbf{x_0}$, $\mathbf{b}$ is filled with the samples $[U_p, V_p, W_p]'$, and $\mathbf{x}$ contains the elements of $\mathbf{F}(\mathbf{x_0}, t)$ and $\mathbf{U}_{\mathbf{x_0}}$ where u_x is $\partial u/\partial x$. The matrices can be written as

$$\mathbf{A} = \begin{bmatrix} 1 & 0 & 0 & X_1 & Y_1 & Z_1 & 0 & 0 & 0 & 0 & 0 & 0 \\ 0 & 1 & 0 & 0 & 0 & 0 & X_1 & Y_1 & Z_1 & 0 & 0 & 0 \\ 0 & 0 & 1 & 0 & 0 & 0 & 0 & 0 & 0 & X_1 & Y_1 & Z_1 \\ 1 & 0 & 0 & X_2 & Y_2 & Z_2 & 0 & 0 & 0 & 0 & 0 & 0 \\ 0 & 1 & 0 & 0 & 0 & 0 & X_2 & Y_2 & Z_2 & 0 & 0 & 0 \\ 0 & 0 & 1 & 0 & 0 & 0 & 0 & 0 & 0 & X_2 & Y_2 & Z_2 \\ & & & & & \vdots & & & & & & \\ 1 & 0 & 0 & X_n & Y_n & Z_n & 0 & 0 & 0 & 0 & 0 & 0 \\ 0 & 1 & 0 & 0 & 0 & 0 & X_n & Y_n & Z_n & 0 & 0 & 0 \\ 0 & 0 & 1 & 0 & 0 & 0 & 0 & 0 & 0 & X_n & Y_n & Z_n \end{bmatrix}, \mathbf{x} \in \mathbb{R}^{12} = \begin{bmatrix} U \\ V \\ W \\ u_x \\ u_y \\ u_z \\ v_x \\ v_y \\ v_z \\ w_x \\ w_y \\ w_z \end{bmatrix}, \mathbf{b} \in \mathbb{R}^{3n} = \begin{bmatrix} U_1 \\ V_1 \\ W_1 \\ U_2 \\ V_2 \\ W_2 \\ \vdots \\ U_n \\ V_n \\ W_n \end{bmatrix} \tag{4}$$

This system can be supplemented with a weighting matrix W that decreases the weight of each sample as its distance from $\mathbf{x_0}$ increases. A penalty c can also be applied to $u_x + v_y + w_z$ to ensure that the flow is not divergent. If this latter penalty is enabled, this problem is solved through Tikhonov regularization with

$$\tilde{\mathbf{x}} = \text{argmin}(\ \|\mathbf{W}(\mathbf{A}\mathbf{x} - \mathbf{b})\|_2^2 + \alpha\|\mathbf{c}\mathbf{x}\|_2^2\ ),\ \tilde{\mathbf{x}} = (\mathbf{A}^{\mathrm{T}}\mathbf{W}^{\mathrm{T}}\mathbf{A} + \alpha\mathbf{c}^{\mathrm{T}}\mathbf{c})^{-1}\mathbf{A}^{\mathrm{T}}\mathbf{W}^{\mathrm{T}}\mathbf{b} \tag{5}$$

In contrast, if the penalty is not enabled, the problem can be split into three one-dimensional problems, allowing for much better performance.

The least-squares formulation has the advantage that, in the event that the variance of the observed data is known, it can be propagated directly to the components of the x vector for the evaluation of uncertainties.

4. Definition of the test cases

The effectiveness of the method is evaluated using synthetic test cases. These comprise images of randomly distributed particles advected in a controlled manner between two time steps. The images were obtained using a high-fidelity in-house PIV image generator, described in Acher et al. (2022) with a density of 0.05 particle per pixel. Two- and three-dimensional configurations can be considered by adjustment of the thickness of the laser sheet and the number and position of the cameras. The particles are massless and are in all cases advected by integrating their trajectory over three-dimensional velocity fields for a given inter-frame time.

A first velocity field is stationary, resulting from the sum of cosines of different wavelengths, the phase of which is set so that the velocity field is solenoidal. This canonical flow contains hyperbolic stagnation points, which are a challenge for correlation-based velocimetry techniques. Its simplicity also allows a convenient assessment of the ability of the different methods to capture the local velocity gradients.

The second velocity field features the characteristic of a turbulent flow. It is generated from the method proposed by Martinez-Sanchis et al. (2021). The mean velocity field has a range of values between 0 and 1 m/s across the vertical direction of the field of view, which covers a distance of approximately 220 mm. The turbulence intensity is 5% relative to 1 m/s, the integral length scale is 100 mm and the Kolmogorv scale is 0.05 mm. For the three-dimensional case, the particles are about 0.5 mm apart. This test case is used to evaluate the different velocimetry techniques in the context of a typical turbulent flow where the smallest scales fall below the resolution of the methods.

5. Application to 2-dimensional cases

The combination of CPD for particle pairing and ALST for Eulerian reconstruction is first compared with a classical 2D2C PIV algorithm.

For this analyse, synthetic images were generated for a 2560×2160 pixels camera capturing a field illuminated by a 0.5 mm thick laser sheet. The particle density was selected to achieve a target value of 0.05 particle per pixel (2.5 pixel between nearest neighbour particles in average). The time between frames is set so that the norm of the maximum displacement of the particles is close to 8 pixels.

The CPD is operated on lists of particles detected from the images by a single pass local peak detection, and localised with a subpixel accuracy through Gaussian fitting.

The first pass of the PIV is performed with a 64 pixels interrogation window, which is decreased to 32 pixels with 75% overlap for the final pass. It results in vectors separated by 8 pixels. The

ALST has been configured to match these dimensions. In particular, the standard deviation of the Gaussian weighting function has been set to 8 pixels, while the search radius is 16 pixels.

A qualitative comparison between the two methods and the imposed velocity field is presented in Figure 2, which depicts the turbulent flow benchmark. In this context, both methods yielded comparable results. However, the field reconstructed with the PIV algorithm exhibited a slight higher degree of blurring. It is also to be noted that neither method is capable of capturing the locally high and low velocity spots that are visible in the reference field. This is because the reference is a snapshot of the velocity field at the intermediate time between the frames. In contrast, the reconstruction can only consider a velocity field that has been averaged over the particle path between the two frames.

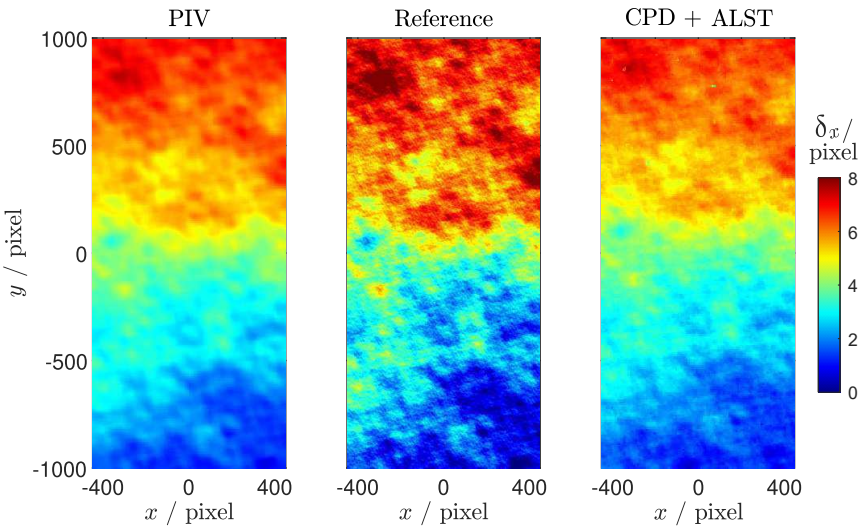

Figure 2. Axial component of the imposed (*Reference*) and reconstructed turbulent particle displacement field with the PIV and 2D CPD+ALST methods.

Figure 3 which is related to the periodic flow can now be analysed for a more quantitative analysis. This velocity field contains hyperbolic stagnation points that present a challenge for PIV reconstruction, as the cross-correlation function computed for interrogation windows that contain such a feature fails to produce a well-demarcated peak. The result of this lack of consistency in the PIV can be observed in the top row of Figure 3, which shows the reconstructed velocity field. The displacement at the positions $x = \pm 200$ pixel and $y = 0$ pixel is indeed not correctly evaluated. The ALST is however to provide a reconstruction that is in good agreement with the reference velocity field.

The bottom row of Figure 3 displays the gradient of the displacement in the x direction. For PIV, the gradient is calculated from the displacement field by finite differences. Consequently, the errors in the reconstruction are amplified by the derivation, as can be observed. With regard to ALST, it is found to provide a relevant reconstruction of the gradient of the displacement, which is a positive finding given that it has been designed for this specific purpose.

These two test cases show that a significant improvement can be obtained in estimating the gradients of a velocity field by applying the compilation of the CPD and the ALST. Nevertheless, the ALST is not as computationally effective as the PIV, as the full process from particle detection to field reconstruction takes three times longer than with PIV with the current implementation. This method is also limited to experiments where the density of the particles is low enough to identify them individually.

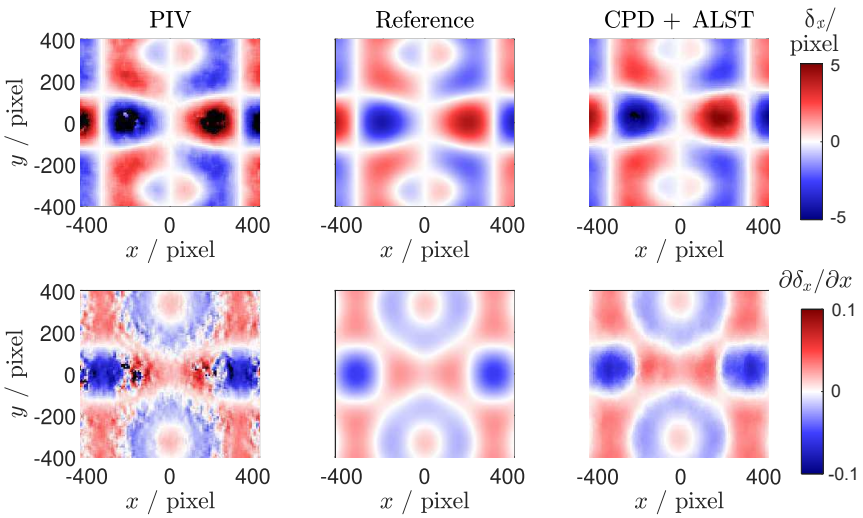

Figure 3. Top row: Axial component of the imposed (*Reference*) and reconstructed periodic particle displacement field with the PIV and 2D CPD+ALST methods. Bottom row: the gradient of the displacement with respect to the x direction.

6. Application to 3-dimensional cases

The main advantage of the proposed method for Eulerian reconstruction is expected to be observed in the context of comparisons with TOMO-PIV, i.e. in three-dimensional problems. The following section presents a comparison between our CPD+ALST method and the classical TOMO-PIV. For the sake of completeness, a comparison is also provided with the results obtained with the two-pulse shake-the-box (STB) method algorithm in combination with the "binning method", both implemented in LaVision Davis 10.2.

The comparison relies of the images obtained from a synthetic experiment involving the periodic and the turbulent flows defined in Section 4. Four 1600 $\times$1200 pixel cameras are even distributed around an axis normal to the measurement volume, which has an approximate dimensions of 300 mm $\times$ 220 mm $\times$ 20 mm. The seeding density is set to achieve 0.05 particle per pixel in the images. This density is chosen because it is the commonly accepted maximum density for the TOMO-PIV, although it could be increased with the CPD+ALST and STB methods (Mercier et al. (2024)). The CPD is applied on lists of particles that have been triangulated from images following

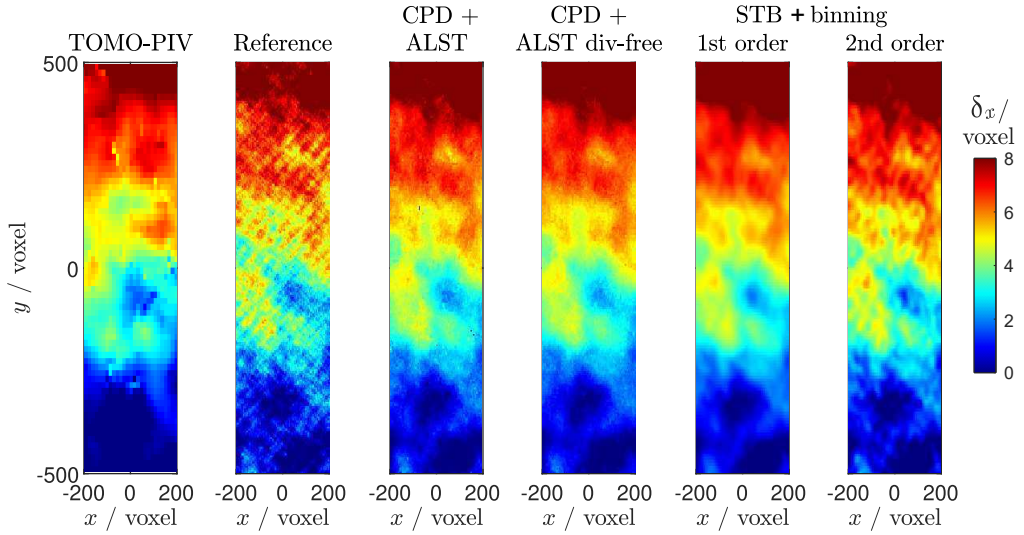

Figure 4. Axial component of the imposed (*Reference*) and reconstructed turbulent particle displacement field with the TOMO-PIV, 3D CPD+ALST, and Shake-The-Box+binning methods.

the procedure described in Thomas et al. (2024).

The comparison involves both the standard ALST and the ALST with penalisation of the divergence, as well as two versions of the binning methods. These are the first- and second-order binning methods, which consist in fitting the local velocity by respectively a first and a second order polynomial. In essence, both ALST and first-order binning are similar insofar as they evaluate both the velocity and its first derivatives. The second-order binning additionally computes the second derivative, which is expected to better resolve regions where velocity field exhibits large curvature.

The TOMO-PIV is performed following a volume reconstruction using the BI-MART method (see Thomas et al. (2014)). The first interrogation volume is 96 voxel large, and it is iteratively reduced to the a final size of 32 voxel. Shake-The-Box and CPD are applied with default parameters. The dimensions involved in ALST and binning are set as small as possible while maintaining stability.

A first qualitative comparison is performed in Figure 4 for the turbulent test case. TOMO-PIV is found to have poor performance compared to all other methods, including a lack of resolution and the presence of numerous artefacts. In contrast, the second-order binning is the most appropriate approach for reconstructing the fine scales that appear as strikes in the imposed velocity field. First-order reconstruction methods have similar performance. However, CPD+ALST tends to produce a less smooth field than first-order binning. It is not clear whether this is the result of higher resolution of the CPD+ALST or whether it is mostly noise. Furthermore, the penalisation of the divergence has only a marginal effect on the reconstructed fields. It seems that it adds some robustness to the process, which in turn leads to the removal of the few spurious vectors that can be found in the raw ALST.

A quantitative analysis of two periodic flows with two different fundamental wavelengths of 300

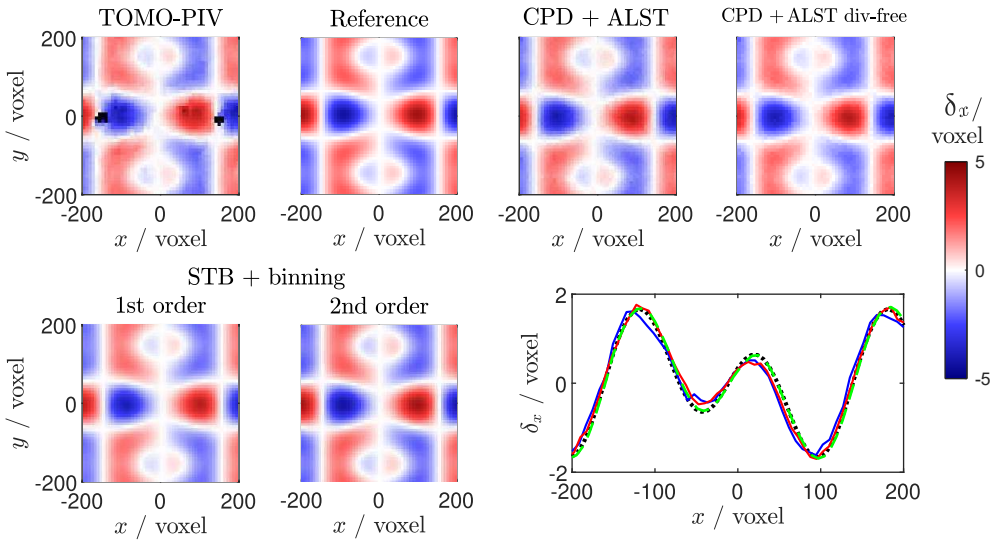

Figure 5. Axial component of the imposed (*Reference*) and reconstructed large wavelength periodic particle displacement field with the TOMO-PIV, 3D CPD+ALST, and Shake-The-Box+binning methods. The graph shows the profile at the constant $y = 150$ for the reference ($\cdots$), the TOMO-PIV (—), the div-free ALST (—), and the 2nd-order binning (– –).

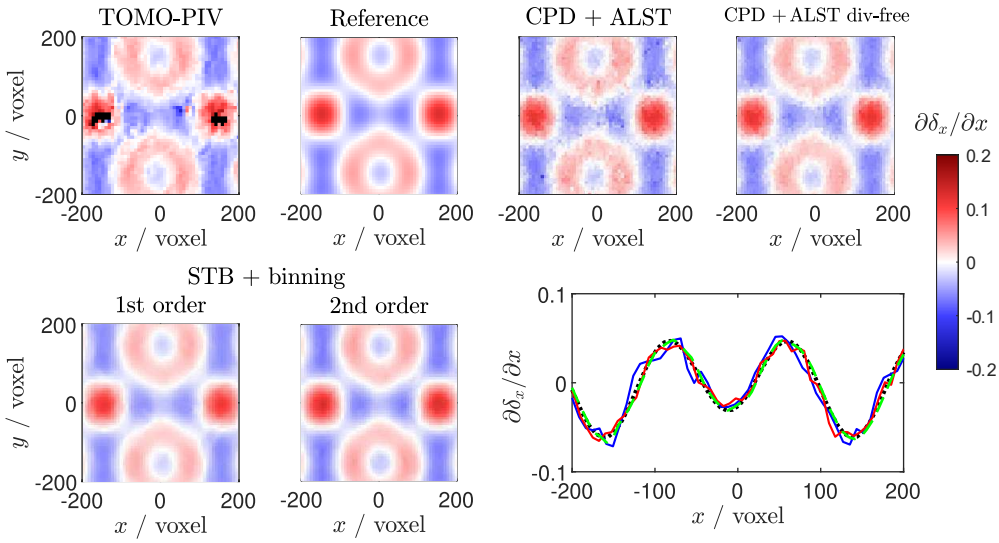

Figure 6. Gradient with respect to the x direction of the axial component of the imposed (*Reference*) and reconstructed large wavelength periodic particle displacement field with the TOMO-PIV, 3D CPD+ALST, and Shake-The-Box+binning methods. The graph shows the profile at the constant $y = 150$ for the reference ($\cdots$), the TOMO-PIV (—), the div-free ALST (—), and the 2nd-order binning (– –).

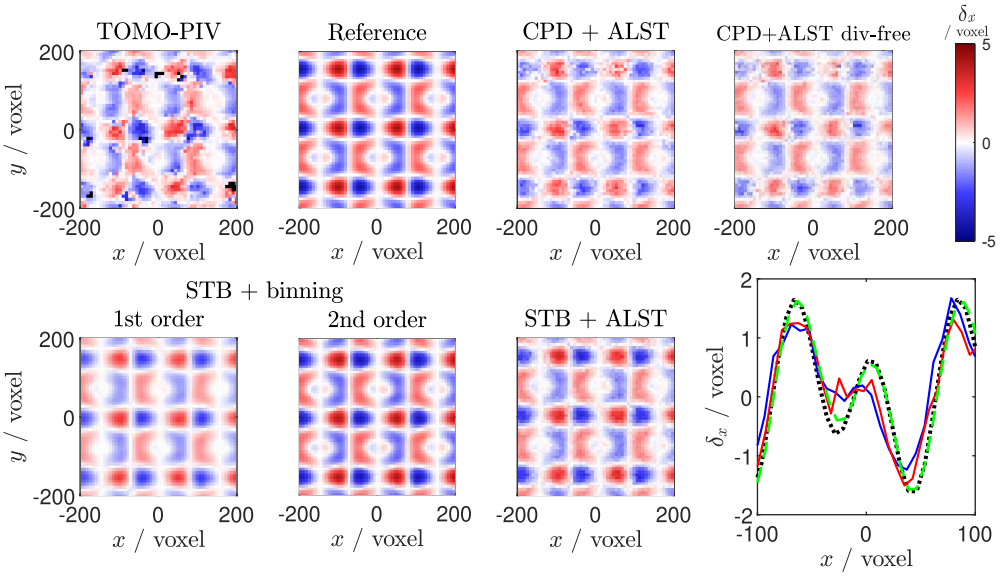

Figure 7. Axial component of the imposed (*Reference*) and reconstructed short wavelength periodic particle displacement field with the TOMO-PIV, 3D CPD+ALST, and Shake-The-Box+binning methods. The graph shows the profile at the constant $y = 150$ for the reference ($\cdots$), the TOMO-PIV (—), the div-free CPD+ ALST (—), and the 2nd-order binning (– –).

and 150 voxel respectively is proposed. The displacements computed by the different methods are shown in Figures 5 and 7 for the two wavelengths, and the gradients of the displacement δ_x with respect to the x direction are given in Figures 6 and 8. For the 300 pixel case, only the TOMO-PIV shows difficulties in reconstructing the field at the location of the hyperbolic stagnation points. The other methods all show very similar results with a slightly higher level of noise for the ALST, especially without the divergence-free condition.

However, the 150 pixel case is more challenging for both TOMO-PIV and CPD+ALST. Indeed, CPD+ALST tends to underestimate the displacement in the region where the flow has the greatest curvature and is noisy along the $y = 150$ voxel line. The first-order binning of the STB traces also suffers from displacement underestimation, but is overall smoother than the CPD+ALST. In contrast, the second order binning is able to reconstruct the reference flow almost perfectly. In an attempt to determine whether the deficiencies of our method were due to the pairing step with CPD or the ALST reconstruction, we also applied the ALST to the list of pairs determined for the STB. The result of this process is also presented in Figures 7 and 8. The accuracy of the reconstructed field with this combination is found to be intermediate between the first- and second-order binning of the same pairs from STB. This implies that the poor reconstruction in some regions is due to the CPD missing a significant number of pairs. As for ALST, provided the input pairs are of good enough quality, it is found to preserve the flow structure better than first-order binning, while both are based on an affine approximation of the displacement field.

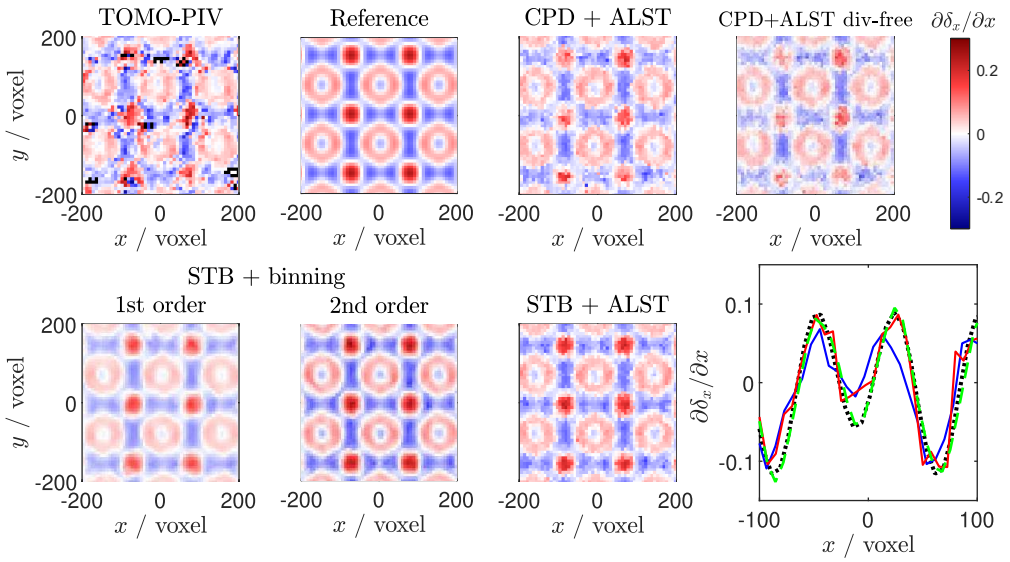

Figure 8. Gradient with respect to the x direction of the axial component of the imposed (*Reference*) and reconstructed short wavelength periodic particle displacement field with the TOMO-PIV, 3D CPD+ALST, and Shake-The-Box+binning methods. The graph shows the profile at the constant $y = 150$ for the reference ($\cdots$), the TOMO-PIV (—), the div-free ALST (—), and the 2nd-order binning (– –).

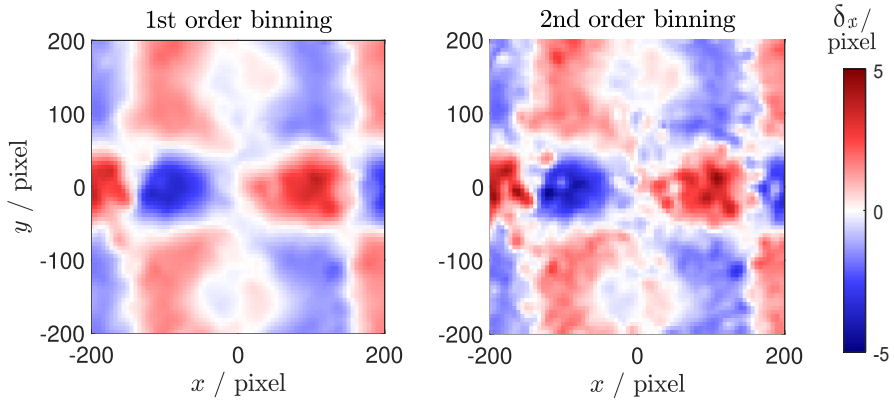

Figure 9. Comparison between the reconstruction displacement field of the large wavelength periodic field with the first-order and the second-order, in the context of dense particle images (0.1 ppp), and with maximum allowed triangulation error of 1.5 voxels in the Davis 10.2 IPR.

The downside of second-order binning's ability to resolve small scales is that it tends to amplify noise that arises in harsher conditions, including higher particle density and higher triangulation error. This is demonstrated in Figure 9 that shows the reconstruction for the same flow as in Figure 5, but with a density of 0.1 particles per pixel, and a maximum allowed triangulation error of 1.5 voxels. These conditions may be encountered in a real experiment, and the corresponding effect they have on the two-pulse Shake-The-Box is described in Mercier et al. (2024).

7. Conclusions and Ongoing work

The authors previously demonstrated that the Coherent Point Drift (CPD) method is a solution to the particle pairing problem in the context of two-pulse velocity. However, the results of CPD alone produce a set of discrete tracks that are strongly affected by particle detection errors and cannot be straightforwardly interpolated on a grid. To address this issue, the authors implemented a method to determine a local affine approximation of the displacement field based on the tracks resulting from the CPD. The so-called Affine Least-Squares Transformation (ALST) method allows Eulerian reconstruction with significantly better performance than TOMO-PIV in 3D problems.

The present work demonstrates the ability of CPD+ALST to reconstruct 2D and 3D velocity fields from 2-instants tracks of different nature better than TOMO-PIV. The ALST also compares well with the first-order binning method proposed in the commercial software Davis 10.2, especially when the divergent-free condition is enabled. However, the second-order binning method which is also implemented in Davis, outperforms the ALST providing the particle pairing is accurate enough.

The calculation of the curvature of the velocity field appears to be very effective in improving the quality of the reconstruction. The second derivatives can be taken into account by modifying the ALST in this way, and this will be part of the ongoing work to develop this framework.

Acknowledgments

The authors would like to thank the ERDF of the Nouvelle Aquitaine Region for their financial support to the Grinfil project (Convention P-2020-BAFE-33) as well as the ANR through the France relance plan (Convention ANR-21-PRRD-0001-01) .

References

Acher, G., Thomas, L., Tremblais, B., & David, L. (2022, sep). A new camera model combining an analytical model and a discrete correction to overcome refractive index variation challenges.

Measurement Science and Technology, *33*(12), 125204.

Dabiri, D., & Pecora, C. (2020). *Particle tracking velocimetry* (Vol. 785). IOP Publishing Bristol.

Gesemann, S., Huhn, F., Schanz, D., & Schröder, A. (2016). From noisy particle tracks to velocity, acceleration and pressure fields using b-splines and penalties. In *18th international symposium on applications of laser and imaging techniques to fluid mechanics, lisbon, portugal* (Vol. 4).

Martinez-Sanchis, D., Sternin, A., Sternin, D., Haidn, O., & Tajmar, M. (2021). Analysis of periodic synthetic turbulence generation and development for direct numerical simulations applications. *Physics of Fluids*, *33*(12), 125130. doi: 10.1063/5.0071002

Mercier, B., Gomez, Q., Thomas, L., Tremblais, B., & David, L. (2023). Proof-of-concept study of coherent point drift registration for particle pairing in particle tracking velocimetry. In *15th international symposium on particle image velocimetry* (pp. 1–6).

Mercier, B., Thomas, L., Tremblais, B., & David, L. (2024). A robust pairing method for two-pulse particle tracking velocimetry based on coherent point drift. *Measurement Science and Technology*.

Myronenko, A., & Song, X. (2010). Point set registration: Coherent point drift. *IEEE Transactions on Pattern Analysis and Machine Intelligence*, *32*(12), 2262-2275.

Myronenko, A., Song, X., & Carreira-Perpiñán, M. (2006). Non-rigid point set registration: Coherent point drift. In B. Schölkopf, J. Platt, & T. Hoffman (Eds.), *Advances in neural information processing systems.* MIT Press.

Novara, M., Schanz, D., & Schröder, A. (2023). Two-pulse 3d particle tracking with shake-the-box. *Experiments in Fluids*, *64*(5), 93.

Raffel, M., Willert, C. E., Scarano, F., Kähler, C. J., Wereley, S. T., & Kompenhans, J. (2018). *Particle image velocimetry: a practical guide*. springer.

Sperotto, P., Pieraccini, S., & Mendez, M. A. (2022, jun). A meshless method to compute pressure fields from image velocimetry. *Measurement Science and Technology*, *33*(9), 094005.

Thomas, L., Mercier, B., Tremblais, B., & David, L. (2024). Coupling coherent point drift and affine least-squares transformation to build trajectories in tr-ptv. In *21st international symposium on applications of laser and imaging techniques to fluid mechanics, lisbon, portugal.*

Thomas, L., Tremblais, B., & David, L. (2014). Optimization of the volume reconstruction for classical tomo-piv algorithms (mart, bimart and smart): synthetic and experimental studies. *Measurement Science and Technology*, *25*(3), 035303.